Structural and Magnetic Properties of Various Ferromagnetic Nanotubes

By *Xiu-Feng Han,* Shahzadi Shamaila, Rehana Sharif, Jun-Yang Chen, Hai-Rui Liu,* and *Dong-Ping Liu*

The structural and magnetic properties of ferromagnetic nanotubes fabricated by a low cost electrodeposition method are investigated. The fabrication of various elemental ferromagnetic materials are described, such as Fe, Co, and Ni, and ferromagnetic alloys, such as NiFe, CoPt, CoFeB, and CoCrPt nanotube arrays, in aluminum oxide templates and polycarbonate membranes with different diameters, wall thicknesses, and lengths. The structural, magnetic, and magnetization reversal properties of these nanotubes are investigated as a function of the geometrical parameters. The angular dependence of the coercivity indicates a transition from the curling to the coherent mode for the ferromagnetic nanotubes. The results show that nanotube fabrication allows the outer and inner diameter, length, and thickness of the nanotubes to be tuned systematically. The magnetization processes of ferromagnetic nanotubes are influenced by the wall thickness.

1. Introduction

An exciting area in materials science is the study of the fabrication of nanostructures such as nanowires and nanotubes because of their potential applications in fields as diverse as optics, electronics, catalysis, magnetism, electrochemistry, information processing, magnetic recording media, etc. An ideal ultrahigh-density recording medium would have a nanostructure with magnetically isolated small grains. The development of magnetic recording media is limited by the super-paramagnetic limit. To overcome this limitation either the effective anisotropy of the material or the thickness of the nanostructures can be increased, that is, using nanocylinders instead of nanodots. Ferromagnetic nanotubes are suggested as a medium for achieving this objective.

Many techniques have been developed for the synthesis of nanotubes, such as thermal decomposition of precursors, hydrothermal synthesis, atomic layer growth, and template-based electrochemical deposition. Among the different strategies for nanotube fabrication, template-based growth has recently attracted much attention because it is a versatile and inexpensive technique. In particular, the inexpensive formation of periodically ordered nanotubes with a periodicity below 100 nm has triggered extensive research. The size, shape, and structural properties of electrodeposited nanotubes are controlled by the template and electrodeposition parameters. The first report on carbon nanotubes in 1991 by S. Iijima[1] was followed by intense experimental and theoretical research on the fabrication of nanotubes because of their particular significance and prospective applications in nanometer-scale devices, chemical and biological separations, catalysis, biosensors, nano-batteries, magneto-resistive random access memory (MRAM), etc.[2]. Nanotubes of conductive polymers, semiconductors, carbon, and composite materials have been fabricated successfully using alumina membranes or track-etched membranes as templates. In comparison with ferromagnetic nanowires, the advancement of ferromagnetic nanotubes is slow because of the difficulties in fabricating ferromagnetic nanotubes with well-controlled dimensions and morphology. Metallic nanotubes have been fabricated by electrodeposition in chemically modified anodic aluminum oxide (AAO) channels,[3] in commercially available AAO,[4] and track-etched polycarbonate (PC) membranes,[5] that have been modified in chemical solutions or by applying a current.[6] However, these methods result in impurities in the nanotubes. In this report a relatively simple nanotube fabrication method without using any modifying agents is presented. Electrodeposition is one of the few methods that can overcome the geometrical restrictions of inserting metals into very deep nanometric recesses, and by controlling the length of the nanotubes and the wall thickness a vortex domain wall can be formed in the nanotube arrays, which can greatly reduce the interaction between array elements. Polymer ion-track membranes and anodic alumina present a number of advantages which makes them suitable for the fabrication of high aspect-ratio nanotubes. In PC membranes, pore sizes ranging from 5 nm to 3 μm can be obtained but they are randomly distributed. Pore densities can be as high as 10^9 pores cm^{-2}. Anodic alumina membranes are prepared by electrochemical oxidation of an Al sheet in acidic solution. Different acids, such as sulfuric acid, oxalic acid, and phosphoric acid can be used for anodization. In practice, sulfuric acid is used to prepare AAO templates with very

[*] Prof. X. F. Han, Dr. S. Shamaila, Dr. R. Sharif, J. Y. Chen, H. R. Liu, D. P. Liu
Beijing National Laboratory for Condensed Matter Physics
Institute of Physics, Chinese Academy of Sciences
Beijing 100190 (China)
E-mail: xfhan@aphy.iphy.ac.cn

DOI: 10.1002/adma.200901065

small pore diameters ranging from 3 nm to about 50 nm, and phosphoric acid is used to fabricate templates with larger pore diameters (>100 nm). Oxalic acid is used to make AAO templates with intermediate pore diameters. The template approach represents an interesting path towards the preparation of nanotubes with controlled morphological properties mainly because by appropriate choice of host templates the shape and dimension of the prepared structures can precisely be determined.

A brief overview of state-of-the-art nanotube fabrication is presented. In the first part of the work, template fabrication, nanotube growth, and fabrication is elaborated. In the second part, the main attention is dedicated to functional nanotube arrays and their special tunable magnetic properties, such as the magnetization reversal mechanism. Magnetic measurements, numerical simulations, and analytical calculations on such tubes have identified two main states: an in-plane magnetic ordering, namely the flux closure vortex state, and a uniform state with all the magnetic moments pointing parallel to the axis of the tube. It is important to establish the method and conditions for reversing the orientation of the magnetization. Although the reversal process has been extensively studied for ferromagnetic nanowires, the equivalent phenomenon in nanotubes has been poorly explored so far in spite of some potential advantages over solid cylinders. Nanotubes exhibit a core-free magnetic configuration leading to uniform switching fields, guaranteeing reproducibility, and because of their low density they can float in solutions, making them suitable for applications in biotechnology. Since coercivity is an important ferromagnetic material property, many researchers still use it as a phenomenological rule. Different magnetization reversal modes can give different angular dependences of the coercivity, so the measurements of coercivity $H_c(\theta)$ curves where θ is the angle between the applied field and the long axis of the tubes provides helpful information about the reversal mechanism.

2. Phenomenology of AAO Template and Nanotubes

2.1. Fabrication of AAO and Nanotubes

We fabricated the anodic oxide templates as follows: a high-purity (99.999%) aluminum (Al) foil was ultrasonically degreased in trichloroethylene for 5 min, and etched in 1.0 M NaOH for 3 min at room temperature (RT). It was then electropolished in a mixed solution of $HClO_4/CH_3CH_2OH = 1{:}4$ (v/v) for 3 min with a constant potential of about 12 V. To obtain highly ordered pores, a two-step anodization was used. In the first anodization step the Al foil was anodized at 0 °C and 40 V dc in 0.3 M oxalic acid for nanotube diameters of 40 nm; at 0 °C and 110 V dc in 5% H_3PO_4 for nanotube diameters of 200 nm; and for about 12 h to form textures on the Al surface. The resulting aluminum oxide layer was then removed by immersing the anodized Al into a mixed solution of 0.4 M chromic acid and 0.6 M phosphoric acid solution at 60 °C. Subsequently, the samples were re-anodized for different periods of time under the same anodization conditions as in the first step. These self-assembled AAO templates were used to fabricate different types of nanotube by electrochemical deposition.

Ferromagnetic nanotubes were fabricated in three kinds of templates: self-assembled AAO (home made), commercially available AAO membranes, and PC membranes. The AAO templates were pre-annealed in air at 100 °C in order to remove moisture from the templates. A conductive layer with a small thickness was sputtered on one side of the AAO and PC template for electrical contact. Electrodeposition was performed in a three-electrode cell under constant voltage at room temperature, where the sputtered conducting layer served as the working electrode, a saturated calomel electrode (SCE) as the reference, and a graphite pole as the counter electrode. The electrolytes contained the salts of the desired metals in appropriate ratios in deionized water. Different lengths of nanotubes were obtained by adjusting the time of the electrodeposition. Different wall thicknesses of the nanotubes were obtained by adjusting the thickness of the working electrode layer.

The morphology and length of the nanotubes was characterized by scanning electron microscopy (SEM). The structural analysis of the ferromagnetic nanotubes was obtained from transmission electron microscopy (TEM) and X-ray diffraction (XRD). The composition was analyzed by induced-coupling plasma atomic emission spectrometer (ICP) combined with chemical analysis and energy dispersive spectrometry (EDS), SEM, and TEM. The magnetic properties of the samples were tested by a vibrating sample magnetometer (VSM) and superconducting quantum interference device (SQUID).

2.2. Morphology of AAO and Ferromagnetic Nanotubes

The fabricated AAO templates contain self-assembled uniform pore arrays with quasi-hexagonal ordering. As an example, Figure 1A shows the AFM top view of a home-made AAO template prepared by two-step anodization in (0.3 M) oxalic acid, with a diameter equal to 40 nm and pore density of about 6.4×10^{11} pores cm^{-2}. Figure 1B shows an SEM image of the home-made AAO template anodized in 5% phosphoric acid with a diameter of ca. 200 nm. The average center-to-center spacing (D_i) and pore diameter (d) depend on the anodization conditions and the electrolyte used for anodization. Generally, the pore diameter of the AAO film increases with increasing anodization voltage, and the length (L) of the pores increases with increasing time of anodization. By using a two-step anodization in different electrolytes, we can fabricate highly ordered and uniform AAO templates with a wide range of diameters and lengths. We have used these self-assembled AAO templates to fabricate various kinds of nanotube arrays by electrochemical deposition. Figure 1C–F shows the schematic diagrams for the growth of magnetic nanotubes by electrodeposition. Figure 1C is the schematic diagram of the template. Prior to deposition, a thin gold layer is sputtered on one side of the template to serve as a working electrode for the deposition of the nanotubes. This thin layer covered the pore walls of the templates, leaving the orifices open (Fig. 1D). The working electrode is connected to the negative potential in the electrolyte solution containing the charged metal ions. By applying an appropriate potential for

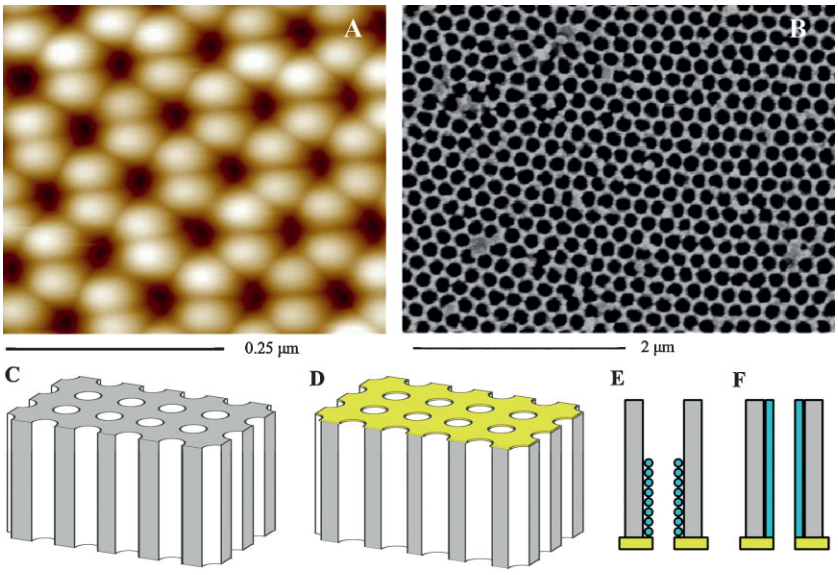

Figure 1. A) AFM top view of home-made AAO templates (anodized in 0.3 M oxalic acid solution) with diameter, *d* ca. 40 nm, and B) SEM image of home-made AAO templates (anodized in 5% H_3PO_4 solution) with diameter, *d* ca. 200 nm. C–F) Schematic diagrams for the growth of magnetic nanotubes by electrodeposition. C) Schematic of the bottom side of the template. D) Thin conducting (Au or Cu) layer sputtered on the bottom side of the template to serve as the working electrode for the nanotubes. E) Accumulation of positively charged ions along the pore walls. F) Parallel growth of metals along the pore walls, producing the nanotube structure.

different metals, positively charged ions accelerated towards the working electrode at the bottom of the pores and accumulated along the pore walls as illustrated in Figure 1E. These metal ions are reduced here to form solid metal by the electrons supplied from the applied potential. This leads to preferential growth of metals along the pore walls, producing the nanotube structure (Fig. 1F).

Figures 2A–F show the SEM images of nanotubes made from different materials. Figures 2A–D exhibit: A) Co, B) Ni, C) NiFe, and D) CoCrPt nanotubes. These nanotubes were fabricated in AAO templates and for SEM imaging these were separated by dissolving the alumina layer in NaOH aqueous solution. The average outer diameter *d* of these nanotubes is ca. 200 nm. Figure 2E shows CoFeB nanotubes and Figure 2F shows a TEM image of Co nanotubes fabricated in a PC membrane as template. For SEM and TEM analysis of the nanotubes fabricated in the PC membrane, the nanotubes were separated from the PC template by dissolving the template in chloroform. The average outer diameter of these nanotubes was ca. 400 nm. These images prove that nanotubes made from several materials with different diameters, lengths, and wall thicknesses can be fabricated by using templates with different diameters. Since the nanocylinders are characterized geometrically by their length (*L*), external and internal diameter (*d* and *a*), respectively, and wall thickness (t_w), where $t_w = 0$ results in nanowires and $t_w > 0$ results in a nanotube geometry. The wall thickness distinguishes nanotubes from nanowires and strongly affects the magnetization reversal mechanism and thereby the overall magnetic behavior.[7] These results reveal that nanotubes with a wide range of diameters, lengths, and wall thicknesses can be fabricated by a low-cost electrodeposition method.

3. Properties of Ferromagnetic Nanotubes

3.1. Structure of Ferromagnetic Nanotubes

The composition of the nanotubes was analyzed by ICP combined with chemical analysis and EDX coupled to SEM and TEM imaging. Structural analysis of ferromagnetic nanotubes was carried out by HRTEM and selected-area electron diffraction (SAED) after releasing the nanotubes from the templates. X-ray diffraction was also performed to obtain structural information on the nanotubes. Figure 2F shows a TEM image of some Co nanotubes. The inset shows the diffraction pattern of the nanotubes showing its fcc crystalline structure. Structural analysis allows us to fabricate nanotubes with different crystal structures according to the required applications.

3.2. Magnetic and Magnetization Properties of Ferromagnetic Nanotubes

Table 1 shows the magnetic properties of metal nanotubes consisting of Fe, Co, and Ni in PC and AAO templates, and NiFe, CoPt, CoFeB, and CoCrPt alloy nanotube arrays fabricated in an AAO template by electrodeposition. The magnetic properties of Fe, Co, and Ni nanotubes in PC templates have been published in our previous work.[8] Here, we compare the magnetic properties of pure and alloy nanotube arrays in an AAO template. The intrinsic properties of the different metals and their alloys are distinct, therefore, the demagnetization field ($2\pi M_s$) of the individual nanotubes and the dipolar interaction among the nanotubes will also be different. Thus, a large variation in the values of H_c and *SQ* (Table 1) and in the magnetic hysteresis (*M*–*H*) curves is observed for nanotubes of different materials. For instance, two typical room-temperature *M*–*H* curves of NiFe and CoCrPt nanotubes with the external field applied parallel and perpendicular to the nanotube axis are shown in Figures 3A and B, respectively. The difference between the *M*–*H* curves of these two materials shows the variety of magnetic properties in ferromagnetic nanotubes. Table 1 proves that the remanent squareness (*SQ*) in the perpendicular direction of the presented nanotubes is large when compared to that in the parallel direction, which shows that the easy axis of these ferromagnetic nanotubes is perpendicular to the tube axis.

3.3. Magnetization Reversal Mechanism

Figure 3C shows the angular dependence of H_c at room temperature for CoCrPt nanotubes and nanowires. The two most common magnetization reversal modes can be modeled by coherent rotation or curling. Generally, for magnetic nanowires and nanotubes, the magnetization reversal mechanism depends

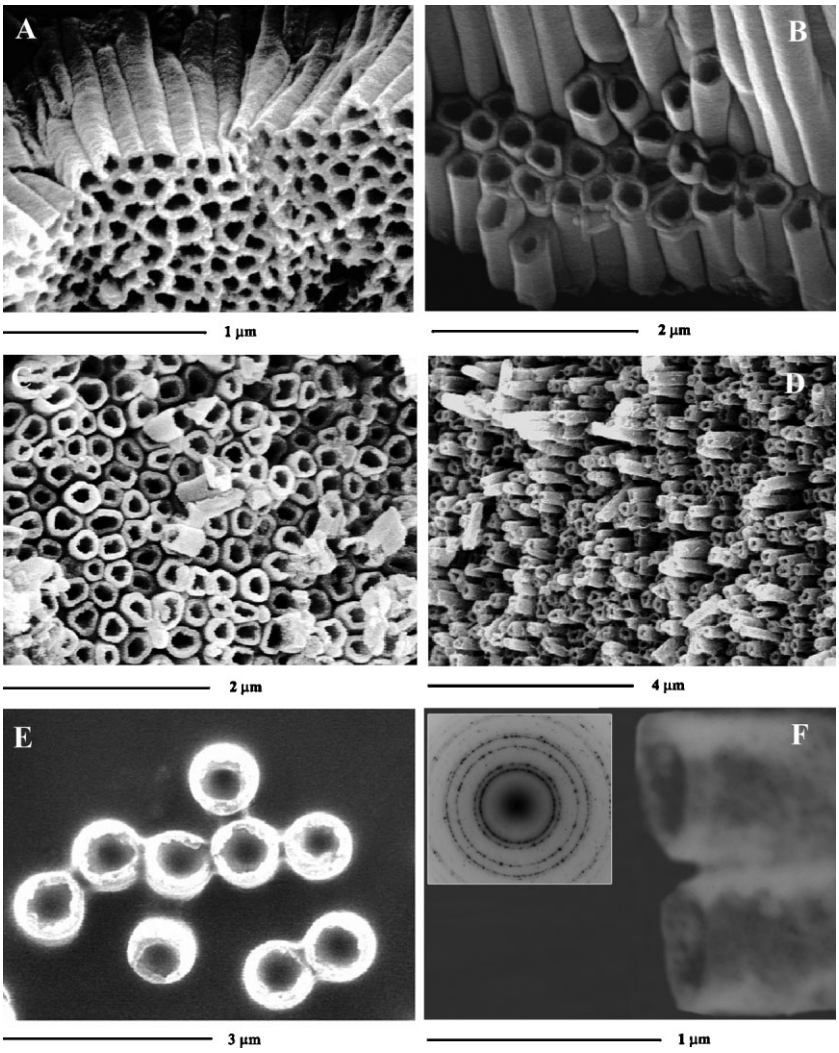

Figure 2. SEM images of isolated A) Co, B) Ni, C) NiFe, and D) CoCrPt nanotubes, separated from the AAO template by dissolving the alumina layer in NaOH aqueous solution. E) SEM image of CoFeB nanotubes fabricated in a PC membrane as a template, the nanotubes were separated from the PC template by dissolving the PC template in chloroform. F) TEM images of isolated Co nanotubes separated from the PC template by dissolving the PC template in chloroform. Inset: Electron diffraction pattern of the Co nanotubes.

upon the outer diameter of the nanocylinders. For a specific material, the critical diameter, d_c, for the transition from coherent rotation to non-coherent rotation is given by:

$$d_c = 2.08(A^{\frac{1}{2}}/M_s) \quad (1)$$

where A is the exchange stiffness and M_s is the saturation magnetization.[9]

For nanowires and nanotubes with diameters larger than the critical diameter, the magnetization reversal process can be described by the curling mode, and H_c decreases with increasing diameter of the nanocylinders. The equation describing the dependence of H_c on the diameter of the nanocylinders in the curling mode is as follows:

$$H_c = \frac{2\pi kA}{M_s}\frac{1}{r^2} + \frac{2K_u}{M_s} \quad (2)$$

where r is the outer radius of the nanocylinders, A the exchange stiffness, K_u the uniaxial anisotropy constant, and k a constant related to the shape of the material (1.08 for an infinite cylinder). The relation between H_c and d_c has already been discussed in detail for nanowires.[10] To a certain extent, this relation can also be generalized for nanotubes in the curling mode. Although the magnetic behavior of nanowires has been intensely investigated, nanotubes have received less attention, in spite of the additional degree of freedom they present; not only the length L and radius r can be varied, but also the thickness of the wall, t_w. Changes in t_w are expected to strongly affect the mechanism of magnetization reversal, and thereby the overall magnetic behavior. Here we explain the magnetization reversal mechanism of CoCrPt nanotubes as compared to that of CoCrPt nanowires. Since the diameter of our samples, $d < M \wedge > 200$ nm, is much greater than the critical diameter (d_c)[11] for coherent rotation, reversal is expected to occur through curling rotation. The curling mode of the reversal mechanism for nanocylinders predicts that

$$H_c = \frac{a(1+a)}{\sqrt{a^2 + (1+a)\cos^2\theta}} H_k \quad (3)$$

Where $a = -1.08(d_c/d)^2$.[12] Equation 3 describes that H_c increases as the angle (θ) increases, whereas the coherent rotation mode predicts that H_c decreases as the angle increases.[11,12] For CoCrPt nanowires H_c increases with increasing angle (θ) from 0° to 90° representing the curling mechanism of

Table 1. Magnetic parameters, coercivity (H_c), and remanent squareness (SQ) of ferromagnetic nanotubes having different lengths (L) in AAO and PC templates with the field applied parallel (//) and perpendicular ($\perp$) to the tube axis.

No.	Composition	L [μm]	H_c //	$H_c^{\perp}$	$SQ^{//}$	$SQ^{\perp}$	Template
1	Fe	6	145	149	0.05	0.22	PC
2	Co	6	158	197	0.11	0.37	PC
3	Ni	6	80	127	0.06	0.31	PC
4	Fe	40	364	163	0.09	0.35	AAO
5	Co	40	115	75	0.03	0.05	AAO
6	Ni	40	111	102	0.16	0.24	AAO
7	$Ni_{64}Fe_{36}$	15	84	68	0.03	0.26	AAO
8	$Co_{90}Pt_{10}$	12	125	177	0.06	0.09	AAO
9	$Co_{80}Fe_{17}B_3$	10	353	108	0.04	0.40	AAO
10	$Co_{75}Cr_{13}Pt_{12}$	10	251	135	0.03	0.13	AAO

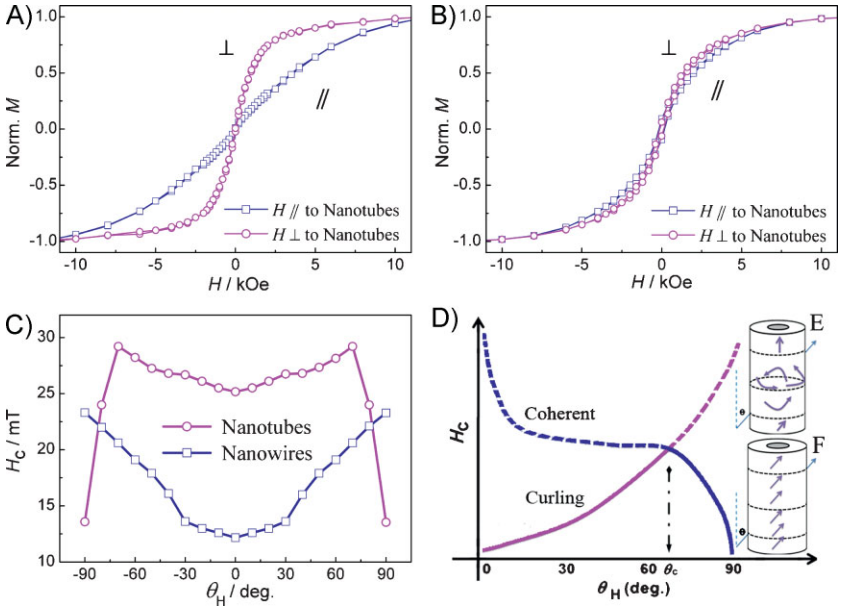

Figure 3. A) *M–H* curve of a NiFe nanotube array. B) *M–H* curve of a CoCrPt nanotube array. C) Angular dependence of the coercivity [*Hc*(θ)] of CoCrPt nanowires and nanotubes where θ is the angle between the field direction and the nanocylinder axis. D) The relative coercive field for angular rotation under curling (purple) and coherent (blue) mode. E, F) Schematic illustrations for the alignment of the magnetic moments during the magnetization reversal process via E) the curling mode and F) the coherent mode.

magnetization reversal. In the case of nanotubes, H_c initially increases with increasing angle up to $\theta \leq \pm 70^\circ$, which is in good agreement with the curling model; however, above this critical angle H_c decreases abruptly expressing an M-type variation. The M-type curve for the nanotubes (Fig. 3C) reveals that at large angles coherent rotation is dominant, while curling happens only for small angles ($\theta \leq \pm 70^\circ$). The distinct geometry of nanotubes presents two dynamic configurations of the magnetic moments with the applied field. When the field angle is small the magnetic moments will align preferably parallel to the tube axis and reversal will take place by curling rotation. At large field angles the moments will align perpendicular to the tube axis and a coherent reversal mode will be observed. Different alignments of the magnetic moments and surface effects are attained in nanotubes because of the influence of the wall thickness, t_w, which causes a transition from a curling to a coherent reversal mechanism for higher angles. The transition angle depends on d and t_w of the nanotubes as theoretically proven previously for other NTs.[13] Figure 3D shows the general trend of the relative coercive field for angular rotation under a curling (purple) and coherent (blue) mode. Figures 3E and F are the schematic illustrations for the moment's alignment during the magnetization reversal process in the presence of the exchange magnetostatic field and crystal anisotropy via E) the curling mode and F) the coherent mode. Our experimental data is in accordance with the trend given in Figure 3D. At finite temperatures, the process of magnetization reversal can be viewed as the overcoming of a single energy barrier (E_B). In an array with all the nanotubes initially magnetized in the same direction the magnetostatic interaction between neighboring tubes favors the magnetization reversal of some of them. A reversing field aligned opposite to the magnetization direction lowers the energy barrier, thereby increasing the probability of switching. Thermal fluctuations can allow the magnetization of a sample to surmount the energy barrier and switch from one stable direction to the other. The dependence of the applied field on the energy barrier is often described by the expression

$$E_B = U(1 - H/H_{c0})^m \quad (4)$$

where U is E_B at zero applied field, H is the applied field, and H_{c0} is the field needed to overcome the energy barrier at zero temperature. For nanowires and nanotubes m is in general equal to 3/2, which is a natural result of the non-symmetrical energy landscape. A linear-field dependence of E_B is also sometimes employed but there is little theoretical justification for such behavior. In short, the magnetization reversal in nanotubes can be determined by the angular dependence of the coercive field in ordered arrays of ferromagnetic nanotubes. A transition between two different modes of magnetization reversal, from curling for small angles, to coherent for large angles, is responsible for the M-type behavior of the coercivity as a function of the field angle. These results show that the magnetic properties can be changed by modifying the geometry. Further adjustments of the deposition time results in lengths as small as 30 nm or even smaller. The nanotubes prepared by this low-cost method offer attractive options in a diverse range of applications, in particular for high-density magnetic recording devices, magnetic random access memory, and magnetic-field sensors.

4. Outlook

Magnetic media fabricated by common nanofabrication techniques can meet the need of controllable grain size but mostly at very high cost. However, these techniques are not stable for grain sizes under 100 nm, while electrodeposition offers a low-cost and simple way to fabricate nanotubes below 100 nm or even smaller. In this article, nanotubes prepared by the electrodeposition method were examined in detail both experimentally and by theoretical analysis. Ferromagnetic nanotubes were synthesized through the electrodeposition method, which proves to be an efficient method to synthesize high-quality, and uniformly distributed nanocylinders in nanoporous templates. The density of the nanotubes can be controlled by modifying the template pores according to the desired application.

This article also gives a comparison of the structural and magnetic properties of ferromagnetic nanotube arrays consisting of elemental Fe, Co, Ni, as well as nanotubes prepared from their

alloys, such as NiFe, CoPt, CoFeB, and CoCrPt using AAO and PC templates. Geometry-dependent magnetization reversal for the nanotubes is reported and discussed in detail, especially the angular-dependent coercivity (H_c) behavior, and compared with that of nanowires. Varying the cylinder geometry different magnetic switching modes are obtained. A curling mode magnetization-reversal mechanism is perceived for CoCrPt nanowires on the basis of angular dependence of the coercivity. For nanotubes a transition from a curling to a coherent reversal process is observed as a function of the angle of the applied magnetic field. For the present nanotube arrays, we could easily control the length, diameter, and tube-wall thickness, as well as the morphology and size distribution. Our electrodeposition method is suitable for future applications in perpendicular recording media. The desired geometry for nanotubes with a wide range of diameter, thickness, and length can be adopted for potential applications such as short nanotubes (nanorings) for patterned recording media,[14] spin-torque transfer (STT) MRAM, and nanoring MRAM.[2,15]

Acknowledgements

The project was supported by the State Key Project of Fundamental Research from the Ministry of Science and Technology (MOST, No.2006CB932200) and the National Natural Science Foundation (NSFC No. 10874225 and 50721001). X.-F.H. thanks the partial support of NSFC-Australia DEST (CH070060), the K. C. Wong Education Foundation, Hong Kong, and the Microfabrication Center of the Institute of Physics. This article is part of a Special Issue on research at the Institute of Physics, Chinese Academy of Sciences.

Published online:

[1] S. Iijima, *Nature* **1991**, *354*, 56.
[2] X. F. Han, Z. C. Wen, H. X. Wei, *J. Appl. Phys.* **2008**, *103*, 07E933.
[3] M. Steinhart, Z. H. Jia, A. K. Schaper, R. B. Wehrspohn, U. Gosele, J. H. Wendorff, *Adv. Mater.* **2003**, *15*, 706.
[4] J. Bao, C. Tie, Z. Xu, Q. Zhou, D. Shen, Q. Ma, *Adv. Mater.* **2001**, *13*, 1631.
[5] F. Tao, M. Guan, Y. Jiang, J. Zhu, Z. Xu, Z. Xue, *Adv. Mater.* **2006**, *18*, 2161.
[6] D. Li, R. S. Thompson, G. Bergmann, J. G. Lu, *Adv. Mater.* **2008**, *20*, 1.
[7] J. Escrig, R. Lavin, J. L. Palma, J. C. Denardin, D. Altbir, A. Cortes, H. Gomez, *Nanotechnology* **2008**, *19*, 075713.
[8] R. Sharif, S. Shamaila, M. Ma, L. D. Yao, R. C. Yu, X. F. Han, M. Khaleeq-ur-Rahman, *Appl. Phys. Lett.* **2008**, *92*, 032505.
[9] H. Zeng, R. Skomski, L. Menon, Y. Liu, S. Bandyopadhyay, D. J. Sellmyer, *Phys. Rev. B* **2002**, *65*, 134426.
[10] S. Shamaila, R. Sharif, S. Riaz, M. Ma, M. Khaleeq-ur-Rahman, X. F. Han, *J. Magn. Magn. Mater.* **2008**, *320*, 1803.
[11] L. Sun, Y. Hao, C. L. Chien, P. C. Searson, *IBM J. Res. Dev.* **2005**, *49*, 79.
[12] G. C. Han, B. Y. Zong, P. Luo, Y. H. Wu, *J. Appl. Phys.* **2003**, *93*, 9202.
[13] J. Escrig, P. Landeros, D. Altbir, E. E. Vogel, P. Vargas, *J. Magn. Magn. Mater.* **2007**, *308*, 233.
[14] M. Albrecht, A. Moser, C. T. Rettner, S. Anders, T. Thomson, B. D. Terris, *Appl. Phys. Lett.* **2002**, *80*, 3409.
[15] Z. C. Wen, H. X. Wei, X. F. Han, *Appl. Phys. Lett.* **2007**, *91*, 122511.